Korean J. Chem. Eng., 37(10), 1810-1820 (2020)
DOI: 10.1007/s11814-020-0581-7

pISSN: 0256-1115
eISSN: 1975-7220

Microchip sensor of PdO-NiO electrode for H_2O_2 sensing fabricated with the UV photolithography

Yong Seok Kim, Tae Kyong Yoo, and Chan-Hwa Chung†

School of Chemical Engineering, Sungkyunkwan University, Suwon 16419, Korea
(*Received 24 February 2020 • Revised 4 May 2020 • Accepted 15 May 2020*)

Abstract−An electrochemical microchip sensor was fabricated through the photolithographic process. The metal paste used in the micro-pattern of the sensor chip contained dendritic and spherical Ag-coated Cu powders, which decreased the electrical resistance of the pattern down to 25.69 Ω·cm by forming a network for electron transfer between particles. The electrode materials were dendritic palladium oxide-nickel oxide powders that showed dramatically high surface area. Also, a synergetic effect on the sensing performance between palladium oxide and nickel oxide was observed. The formation of micro-pattern was investigated through optical microscope and field-emission scanning electron microscope. The body resistance of the conductive paste was calculated using the 4-point probe technique, and the electrochemical characteristics of the sensor were analyzed by cyclic voltammetry and chronoamperometry. The fabricated sensor chip exhibited sensing performance for hydrogen peroxide detection with high sensitivity of 641.75 μA mM^{-1} cm^{-2} in a dynamic range between 50 μM and 13 mM. Its long-term stability and high selectivity were also confirmed.

Keywords: Microsensor Chip, Silver-coated Copper, Photolithography, Hydrogen Peroxide, Palladium Oxide-nickel Oxide

INTRODUCTION

In the fields of environment, health, food, pharmaceutical research and clinical study, one of the most widely recognized issues is the treatment of hazardous components. A countless number of toxic materials exist in each area, but hydrogen peroxide (H_2O_2) should be considered as a primary target because not many toxicants have wider use than hydrogen peroxide. Compared to other numerous toxic materials, hydrogen peroxide shows much greater presence in numerous fields, such as the food industry, pharmaceuticals, clinical, environmental analysis, antiseptics, biochemistry, and other industrial manufacturers [1,2]. Thus, the need for an accurate, sensitive, rapid, and inexpensive way to detect hydrogen peroxide is recognized as an important issue, and many attempts have been made to develop the advanced sensing technology. A number of sensor devices, such as piezoelectric sensors, pyro-electric sensors, and electrochemical sensors, were developed to suggest a breakthrough to this common issue. Among all the different types of sensors, the electrochemical sensor has shown clear superiority over the other kinds; it not only exhibits rapid response and high sensitivity, but also utilizes simple equipment, proving itself as a clear solution against hydrogen peroxide sensing.

Recently, various methods have been applied to fabricate electrochemical sensor devices. Additive printing methods, mainly inkjet printing [4], screen printing [5,6] and 3D printing [7] methods are widely used to manufacture electrochemical sensor devices. However, these methods have a fatal limitation on decreasing the size of the devices. So far, practical micro-patterns formed by print-screen method with metal-paste stay on 70 μm of width length, and it is technically difficult to make patterns with smaller width length [8]. An rising method, which can meet the demands for a smaller-sized pattern, maintaining high sensitivity as a sensor and suitability for mass production, is photolithography. By adopting the photolithographic process into the electrochemical sensor production in forms of compact microchips, the size of the sensor chips can become much smaller than the typical sensors. The width of the patterns on the sensor chips can reach under the level of few tens of micrometers, which cannot be accomplished with the typical screen-printing, inkjet printing and 3D printing methods.

In the fabrication of a microchip sensor by photolithography, the most important materials are the photosensitive paste and the electrode materials. Normally, the photosensitive paste is a complex compound with a metal filler of high electrical conductivity, organic vehicles of liquidity, and some other additives. Among the components, the metal filler occupies the most critical part because it eventually determines the electrical conductivity and stability of devices, forming a network of electron paths by contacting themselves in the paste. Considering electrical conductivity, the pastes composed of novel-metal powders such as gold (Au) and silver (Ag) are common choices. Due to their rarity, value and price, however, it is almost impossible to utilize these novel metals in photosensitive paste under reasonable prices, and thus the need of alternative materials has always been an issue. Copper (Cu) is one of the promising materials that can replace Ag. Copper has high electrical conductivity of 5.96×10^7 S/m with very low price. However, Cu exposed to air is very easily oxidized and changes into Cu_xO, which shows very high electrical resistance compared to pristine copper. One solution is to adopt a core-shell structure. In this case, copper works as the core

†To whom correspondence should be addressed.
E-mail: chchung@skku.edu

material and is protected from oxidation by forming an anti-oxidation shell composed of other metals [9-14].

Several methods have been studied to form the protecting and conducting shell on the surface of core materials. Electro-plating with exterior electricity, vacuum process, electroless plating (ELP) using reducing agents without electricity supply, and chemical reduction process utilizing galvanic displacement reaction (GDR) based on the difference of standard reduction potentials of various metals are representative. Electro-plating and vacuum process are suitable for making shells on various substrates, but they have limitation on industrial application due to their complexity. Although electroless plating was developed which does not require expensive equipment, the reducing agents used in the process, such as hydrazine and formaldehyde, are highly toxic and thus cannot avoid environ-

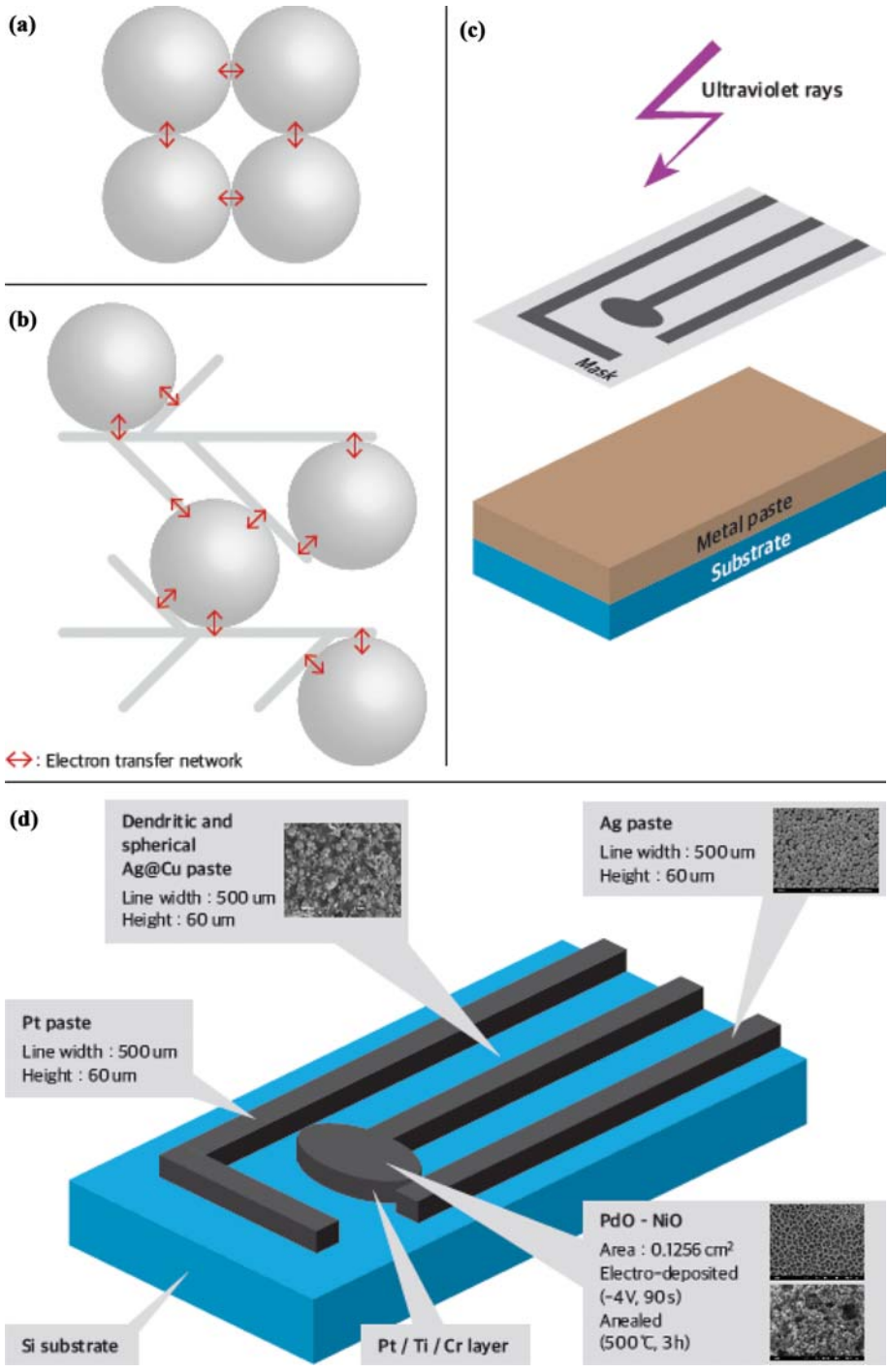

Scheme 1. Schematic diagrams of the electron transfer networks within (a) the spherical Ag@Cu powders and (b) the mixture of dendritic and spherical Ag@Cu powders and the schematic diagrams of (c) a photo-lithography process and (d) the structural scheme of the microchip sensor for H_2O_2 detection prepared in this work.

mental issues [11-13,15]. On the other hand, chemical reduction utilizing the galvanic displacement reaction nearly uses no hazardous materials during the process and forms a relatively uniform and clean shell structure on complex forms of copper powders with a very simple process. In our previous work, Park et al. successfully created the Ag shell on dendritic Cu powders using the galvanic displacement reaction with facile two-step process and characterized the superior electrical conductivity of the obtained Ag-coated Cu (Ag@Cu) powders [16].

Another critical part of the electrochemical sensor chip is the electrode, on which the electrochemical sensing signal is obtained. Various metals or metal oxides, such as platinum, gold, silver, palladium, nickel oxide, iron oxide, titanium oxide, and palladium oxide, have been studied to apply on the H_2O_2 sensor [17-20]. Among all the candidates, the metal oxides have attracted great interest because they are relatively inexpensive and easy to prepare. Especially, palladium oxide (PdO) and nickel oxide (NiO) have been reported as fine sensing materials. Zhu et al. fabricated a sensing electrode with PdO as a potentiometric sensor and discussed the sensing performance against carbon monoxide [21]. Ojani et al. also modified the carbon paste with NiO for hydrogen peroxide sensing and proved the practical usability in determining concentrated hydrogen peroxide by showing the linearity between the oxidation current and the concentration [22].

Not only the electrode materials but also the morphology of the materials is critical in determining the performance of electrochemical sensor, since it is known that the redox reactions between the analytes and the sensors mostly occur on the active adsorption sites of the electro-catalyst at the sensing electrode surface [22-24]. Therefore, the more exposed sites on the electro-catalytic surface obviously provide a higher performance, which is quite important in microchip sensors. Focusing on this aspect, An et al. produced a dendritic palladium electrode for hydrogen peroxide sensing. They prepared the sensor electrodes through electrodeposition process on a dynamic hydrogen-bubble template. The hydrogen-bubble template allowed the electrode materials to have many nano- and micro-sized features or pores and produced specifically large catalytic surface area, which directly affected the sensor performance [25].

In this work, the microchip sensor with the small-sized patterns was fabricated to be used in H_2O_2 detection, of which structural scheme is presented in Scheme 1. The micro-patterning of circuits with the small-sized patterns on the chip substrate was conducted with the photo-lithographic process using a photo-sensitive paste of dendritic Ag@Cu powders. On these micro-patterns of the circuits, the highly porous PdO-NiO sensor electrode was fabricated by electro-deposition of Pd-Ni using a dynamic hydrogen-bubble templating method followed by the annealing process. Here, we monitored and report the role of NiO in the catalytic performance of H_2O_2 detection in the PdO-NiO sensor. The effect of dendritic Ag-coated Cu pastes on the electrical conductivity of photosensitive paste used in this work was also discussed. The micro-patterns were observed using the optical microscope (Bimeince, WM0015000A (S15A) Uplight) and field-emission scanning electron microscope (JEOL, JSM7000F). The resistance of the prepared pattern was measured with a 4-point probe. The physico-chemical properties of the fabricated PdO-NiO were also characterized using X-ray diffraction (Bruker, D8 ADVANCE) and X-ray photoelectron spectroscopy (Thermo, ESCALAB250). Furthermore, the H_2O_2 electrochemical sensing performance of the prepared PdO and PdO-NiO electrodes was analyzed with cyclic voltammetry and chrono-amperometry.

EXPERIMENT

1. Materials

For the fabrication of Ag-coated Cu powders, $CuSO_4 \cdot 5H_2O$ (Daejung chemicals, Korea), HCl (35%, Daejung chemicals, Korea), NaCl (Daejung chemicals, Korea), ethylene diamine tetra acetic acid (EDTA, Sigma-Aldrich), HNO_3 (60%, Daejung chemicals, Korea), NH_4OH (25%, Daejung chemicals, Korea), $N_2H_4 \cdot H_2O$ (80%, Samchun, Korea) were purchased. Silver powders of 1-2 μm were also purchased from Alfa aesar to be used in a reference electrode of the sensor chip.

Cyclosiloxane acrylate (COTEM, Korea), diethylene glycol monoethyl ether acetate (98%, Daejung chemicals, Korea), diphenly (2,4,6-trimethylbenzoyl) phosphine oxide (97%, Sigma-Aldrich) were employed to formulate the photosensitive paste.

In the preparation of sensing electrode, $PdCl_2$ (Kojima Chemicals, Japan), $NiSO_4 \cdot 6H_2O$ (Daejung Chemicals, Korea), and H_2SO_4 (95%, Daejung Chemicals, Korea) were purchased and dissolved in water preparing the aqueous electrolyte for electro-deposition Pd-Ni layer. The phosphate buffer solution (PBS, 0.1 M, pH=7), uric acid (UA), and glucose, dopamine hydrochloride (DA), and ascorbic acid (AA) were obtained from Sigma-Aldrich for the electrochemical H_2O_2 sensing performance of the electrode.

2. Fabrication of Dendritic Cu Powders

Dendritic Cu powders were obtained from a simple galvanic displacement reaction, which is driven by the difference of standard reduction potentials of Al and Cu. First, a commercial Al foil of 8 cm×10 cm was prepared and put into 1 M KOH solution for 5 min to remove oxide layer. The 0.1 M $CuSO_4 \cdot 5H_2O$ was used as the metal source to be reduced into Cu, which was dissolved with 1 M NaCl and 0.2 M HCl electrolyte solution of deionization water (DI). The galvanic displacement reaction occurred when the Al foil was put in the electrolyte. After 30 min of the galvanic displacement reaction, dendritic Cu powders were produced on Al foil. The dendritic Cu powders were rinsed with DI water several times until impurities were completely removed. Once the dendritic Cu powders were collected after filtering, the powders were dried for 12 hours in a vacuum oven at 50 °C [16].

3. Fabrication of Dendritic Ag-coated Cu Powders

For use as metal fillers in a photosensitive paste for circuit patterning in microchip sensors, dendritic Ag-coated Cu (Ag@Cu) powders were prepared as follows. Before coating the dendritic Cu powders with Ag, the pre-conditioning process to remove microscopic oxide layer that may exist on the surface of dendritic Cu powders proceeded. The dendritic Cu powders were dispersed in DI water using an ultra-sonicator. And then, the well-dispersed Cu powders were immersed into a mixture solution of NH_4OH and $(NH_4)_2SO_4$ for 30 min with stirring [16]. After the pre-conditioning step, the oxide layer-free Cu powders were rinsed with DI water several times and put into a base solution with DI water of 200 mL.

The 0.03 M EDTA was then added to base solution as a chelating agent.

The 200 mL of Ag coating solution was prepared with 0.1 M $AgNO_3$ and 0.35 M NH_4OH. Another 200 mL of 0.3 M $N_2H_4{\cdot}H_2O$ contained reducing-agent solution was also prepared. These coating solutions and reducing agent solution were dropped into the Cu-powder dispersed solution. After dropping, the obtained Ag@Cu powders were rinsed with DI water several times and dried again for 12 hours in vacuum at 50 °C.

4. Circuit Patterning by Photolithography

For the patterning of sensor-chip circuits with photolithography, the photosensitive paste was prepared as follows. Metal fillers were either spherical Ag powders or dendritic Ag-coated Cu powders. As an organic binder, cyclosiloxane acrylate copolymer was used with the solvent of diethylene glycol monoethyl ether acetate (ECA), in which diphenyl (2,4,6-trimethylbenzoyl) phosphine oxide (TPO) was added as a photo-initiator. All these materials were mixed with a mixer (Thinky, AR-250) at 2,000 rpm for 3 min. The weight ratio of [metal filler : binder : solvent : photo-initiator] was [5 : 1 : 4 : 0.3] in the mixture of paste. Using this formulated photosensitive paste, the photolithography process proceeded as follows. The prepared paste was coated and pre-baked at 110 °C for 30 min on PET film. Using a UV exposure machine (Opto Finetech, KP-1200), the masked photo-sensitive paste layer was exposed to the UV. The exposed paste was then developed in 2 wt% Na_2CO_3 aqueous solution. After development, the patterned film was post-baked at 110 °C for 30 min.

5. Body Resistivity Measurement of the Developed Photosensitive Paste

The 4-point probe method was used to measure electrical conductivity on the UV-patterned circuits. The resistance value was recorded at a constant current of 20 μA by using a current source (Keithley 6221) and a nano-voltmeter (Keithley 2182A), when a probe was tungsten and the distance between the probes was 1 mm. The body resistivity was calculated according to Eq. (1):

$$\rho = C \times t \times \frac{V}{I} \tag{1}$$

where ρ is body resistance [Ω·cm], C is the correction factor, t is film thickness [cm], V is voltage [V], and I is current [A].

6. Preparation of Nano-structured PdO-NiO Sensor Electrode

The Pt was sputtered on a designated area of 0.1246 cm^2, after the sputtering of thin Ti film as an adhesion layer on the Si substrate. This Pt/Ti/Si substrate was used as a working electrode for Pd-Ni electro-deposition. A platinum plate (1 cm×4 cm) and the Ag/AgCl (1 M KCl) were used as counter electrode and reference electrode, respectively. The Pd-Ni electrode was fabricated by applying a high cathodic over-potential of −4 V for 90 sec in the electrolyte of 10 mM $PdCl_2$, 200 mM $NiSO_4{\cdot}6H_2O$, and 1 M H_2SO_4, which induced the electro-deposition of a dendritic Pd-Ni layer accompanied by hydrogen bubble evolution. Once after the dendritic Pd-Ni layer formation, the annealing process was performed at 500 °C for 3 hours in air to oxidize the Pd-Ni.

7. Fabrication of Sensor-chip Circuits

In the fabrication of sensor-chip circuits, the spherical Ag powders and a mixture of spherical Ag powders and dendritic Ag@Cu powders were used for a circuit line connected to a reference electrode and a working electrode, respectively. Using those metal fillers, photo-sensitive conductive pastes were formulated and printed on an Si wafer. After pre-baking at 110 °C for 30 min, the UV was exposed and the patterns of circuits were developed. To build the counter electrode, Pt powders were mixed with cyclosiloxane acrylate copolymer and ECA, which was also printed on the Si wafer.

8. Characterization

The morphological structure of the PdO-NiO sensor electrode and the dendritic Ag@Cu powders was monitored by field-emission scanning electron microscopy (FESEM, JEOL, JSM7000F), and the size of the powders was analyzed with the particle size analyzer (PSA, Malvern, MS3000_MV&LV). The X-ray diffractometer (XRD, Bruker, D8 ADVANCE) and X-ray photoelectron spectroscope (XPS, Thermo, ESCALAB250) were used to analyze the crystallinity and the chemical composition of the dendritic Ag@Cu powders, respectively. The images of patterned circuits were also obtained by optical microscope (Bimeince, WM0015000A (S15A) Uplight).

9. Electrochemical Measurement of H_2O_2 Sensing Performance

All the electrochemical experiments were performed using an electrochemical workstation (Zahner Elektric, IM6ex, Germany) with three-electrode configuration. The dissolved oxygen in the electrolyte was removed by purging with N_2 for 5 min before all electrochemical measurements. The H_2O_2 sensing performance of the PdO-NiO electrode was characterized by cyclic voltammetry with a scan rate of 20 mV s^{-1} in an electrolyte of 0.1 M PBS, in which the voltage was scanned between −0.8 V and +0.8 V vs. Ag electrode. The sensitivity and the selectivity on the PdO-NiO electrode were also evaluated by chrono-amperometric measurements.

RESULTS AND DISCUSSION

The dendritic Cu powders were obtained from simple galvanic displacement reaction, which is driven by the difference of standard reduction potentials of Al and Cu. [16]. The Al metal plays role of reducing agent in this reaction. At the same time, the H^+ ions were reduced to hydrogen, which is hydrogen evolution reaction, during Cu^{2+} ions were reduced to Cu metal. Due to the interaction between Cu and hydrogen bubbles, the dendritic structures are formed. All the fundamental reactions in the fabrication process of dendritic Cu powders are summarized as follows. First, the spontaneous replacement reaction between Al and Cu^{2+} ion occurs due to the difference of standard reduction potentials as noted in Eqs. (2) and (3):

$$Al^{3+}(aq) + 3e^- \rightleftarrows Al(s), \quad E^o = -1.676\ \text{V vs. SHE} \tag{2}$$

$$Cu^{2+}(aq) + 2e^- \rightleftarrows Cu(s), \quad E^o = 0.340\ \text{V vs. SHE} \tag{3}$$

As a result, the Cu^{2+} was reduced and the metallic Cu was obtained, whereas the Al was dissolved into the electrolyte (cf. Eq. (4)).

$$2Al(s) + 3Cu^{2+}(aq) \rightarrow 2Al^{3+}(aq) + 3Cu(s) \tag{4}$$

At the same time, there is also hydrogen bubble evolution due to the reduction potential difference between Al and proton in the electrolyte as in Eq. (5).

$$2Al(s)+6H^{+}(aq)\rightarrow 2Al^{3+}(aq)+3H_2(g) \quad (5)$$

In the formation of Ag-shell layer on the Cu powders, we used two sequent steps: First is a galvanic displacement reaction between Cu and Ag^{+} ion, and the next is electroless plating using reducing agent of $N_2H_4{\cdot}H_2O$. In the first step, the Ag^{+} ions replaced Cu and deposited as a thin layer of metallic Ag at the shell on the Cu powders due to the difference between the reduction potentials of Cu and Ag^{+} as shown below.

$$2Ag^{+}(aq)+2e^{-}\rightleftarrows 2Ag(s), \quad E^{o}=0.7991\ V\ vs.\ SHE \quad (6)$$

$$Cu^{2+}(aq)+2e^{-}\rightleftarrows Cu(s), \quad E^{o}=0.340\ V\ vs.\ SHE \quad (7)$$

$$2Ag^{+}(aq)+Cu(s)\rightarrow 2Ag(s)+Cu^{2+}(aq) \quad (8)$$

As noticed in Fig. 1, the SEM images show the morphology of the dendritic Ag@Cu powders. The average size of the fabricated dendritic Ag-coated Cu powders is confirmed to be D_{50}=2.831 μm with pore size analyzer as shown in Fig. 2. In the XRD analysis on the fabricated dendritic Ag@Cu powders, the Ag (111), Ag (200), and Ag (220) peaks are evident at 38.0°, 44.3°, 64.5°, whereas Cu (111), Cu (200), and Cu (220) are still presented at 43.2°, 50.3°, and 74.1°, respectively, as shown in Fig. 3. There are no peaks of CuO and Cu_2O, which indicates that Cu was oxidized neither to CuO nor to Cu_2O when a uniform Ag-shell layer was formed.

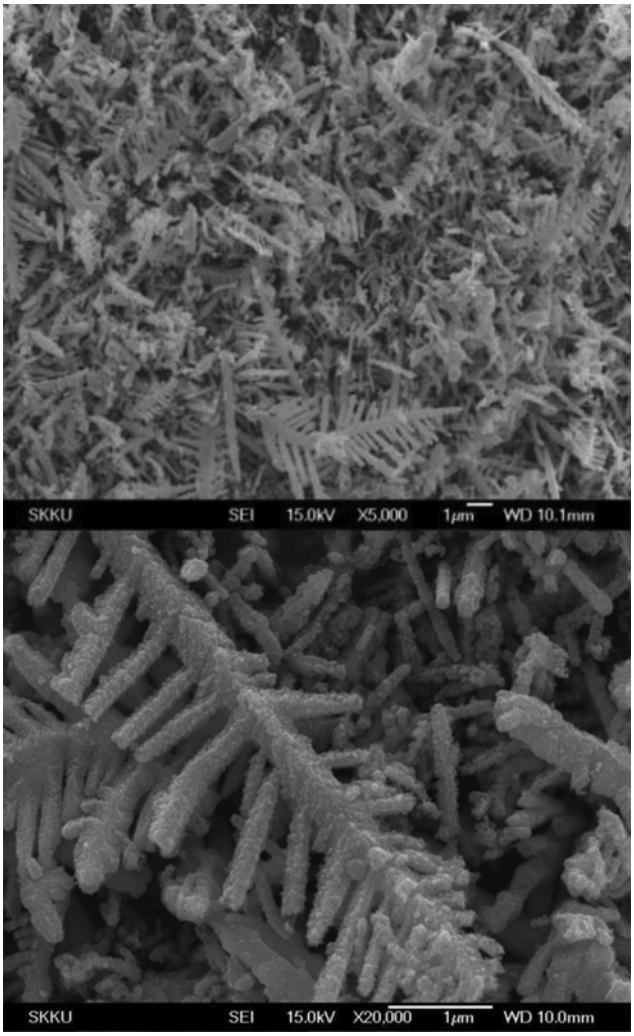

Fig. 1. SEM images of prepared dendritic Ag@Cu powders.

After formulating the photosensitive pastes using dendritic Ag-coated Cu powders, their body resistivity was measured with 4-point probe. All the samples were prepared with the same mixing ratio of metal-filler to organic binder, which is 5 to 1 in wt%, whereas each of the samples contained different amount of dendritic Ag-coated Cu powders in the metal fillers of spherical Ag powders. They were printed and dried on 2 cm×2 cm PET film with an identical thickness of 60 μm. In the estimation of body resistivity, the correction factors in Table 1 were used. In Table 1, *a* is the horizontal length, *d* is the vertical length, and *s* is the distance between the points on the probe, respectively. The detailed calculation followed the Eq. (1) [26].

As presented in Table 2 and Fig. 4, a smaller value of body resis-

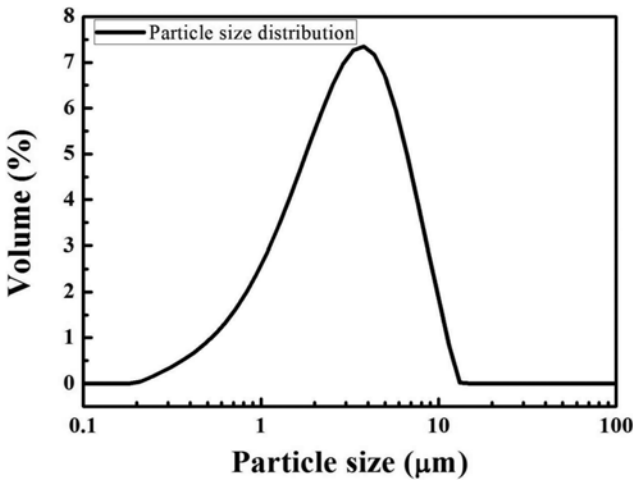

Fig. 2. Particle size distribution of dendritic Ag@Cu powders prepared in this work.

Table 1. Table of correction factors in the estimation of body resistance

d/s	a/d=1	a/d=2	a/d=3	a/d≥4
1.0			0.9988	0.9994
1.25			1.2467	1.2248
1.5		1.4478	1.4893	1.4893
1.75		1.7196	1.7238	1.7238
2.0		1.9454	1.9475	1.9475
2.5		2.3532	2.3541	2.3541
3.0	2.4575	2.7000	2.7005	2.7005
4.0	3.1137	3.2246	3.2248	3.2248
5.0	3.5098	3.5749	3.5750	3.5750
7.5	4.0095	4.0361	4.0362	4.0362
10.0	4.2209	4.2357	4.2357	4.2357
15.0	4.3882	4.3947	4.3947	4.3947
20.0	4.4516	4.4553	4.4553	4.4553
40.0	4.5120	4.5129	4.5129	4.5129
∞	4.5324	4.5324	4.5325	4.5324

Table 2. Body resistivity obtained from the different samples of pasted films with various contents of dendritic Ag@Cu in metal fillers

	Sample 1	Sample 2	Sample 3	Sample 4	Sample 5
Dendritic Ag@Cu content in metal fillers [wt%]	0	33	50	67	100
Body resistance [Ω·cm]	38.46	31.65	29.07	27.02	25.69

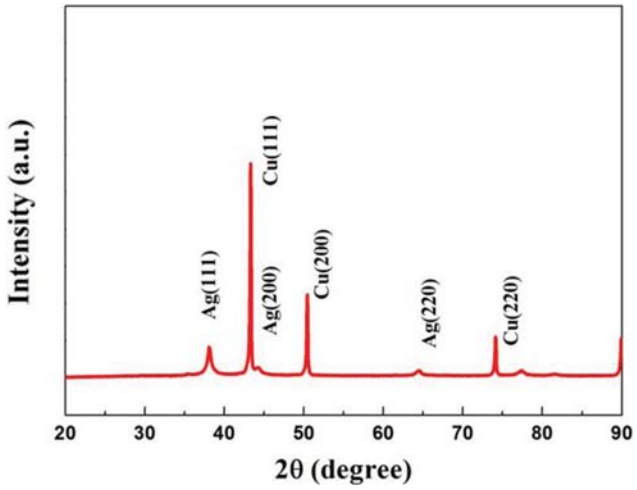

Fig. 3. XRD patterns obtained from dendritic Ag@Cu powders.

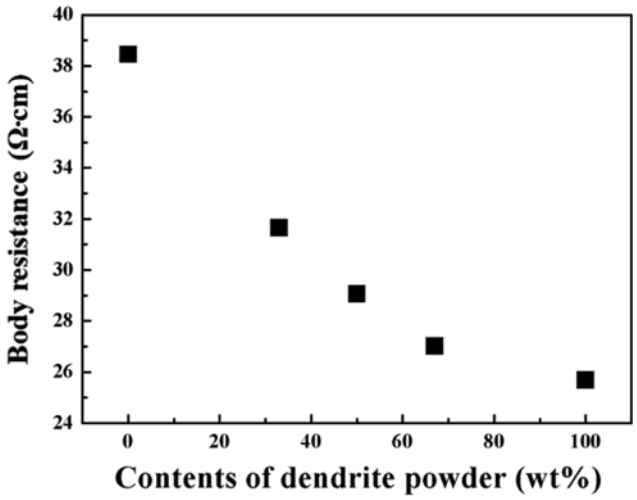

Fig. 4. Changes of body resistance according to the amount of dendritic Ag@Cu powders in metal fillers of photosensitive paste.

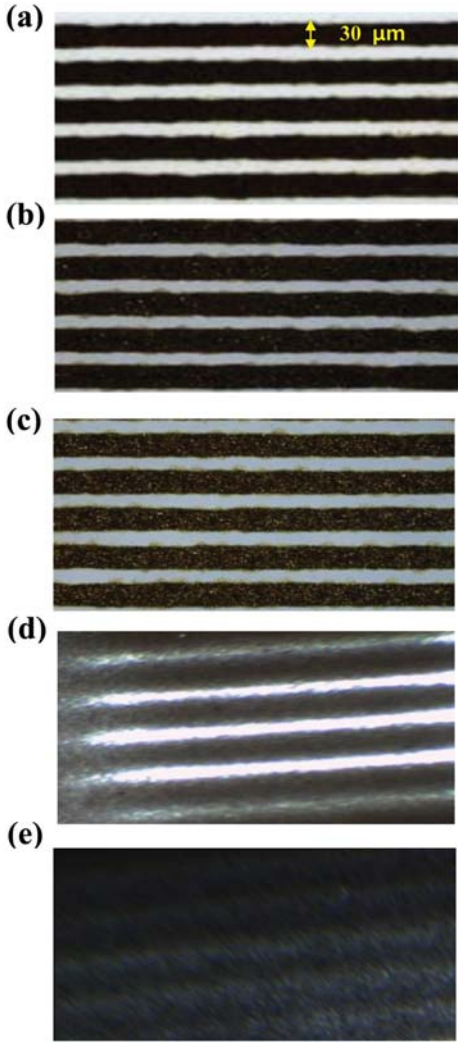

Fig. 5. Optical microscopic images of circuit patterns obtained after the UV photolithography with the paste containing (a) 0 wt%, (b) 33 wt%, (c) 50 wt%, (d) 67 wt%, and (e) 100 wt% of dendritic Ag@Cu powders in metal fillers, respectively.

tivity was obtained as a greater amount of dendritic Ag-coated Cu powders was formulated into the pastes. It is because more networks are formed when more dendritic particles are introduced, which are contacting each other relatively well compared to spherical particles.

For use in circuit chip of the sensor, not only good conductivity but the clearness of the patterning feature is also essential. Fig. 5 shows an optical microscopic image of patterned line, which is obtained after the UV photolithography using the formulated photosensitive pastes with different content of dendritic Ag@Cu powders. In common sense, the UV light is supposed to be scattered more when more dendritic metal particles are included in the pastes, which results in poor patterns. As noticed in Figs. 5(a), 5(b), and 5(c), all the patterns developed well with the 33 wt% and 50 wt% content of dendritic Ag@Cu powders in metal fillers of the paste, which are comparable to those with only spherical Ag powders. As shown in Figs. 5(d) and 5(e), however, the amount of dendritic Ag@Cu powders was too much to develop the patterns clearly when the content of dendritic powders was 67 wt% and 100 wt%. Considering the easiness of the process and the conductivity data, a photosensitive paste with the metal fillers of 33 wt% dendritic Ag@Cu was decided to be the optimum condition for the fabrication of the circuit patterns for a microchip sensor in this work.

For the preparation of H_2O_2 sensing electrode in a microchip

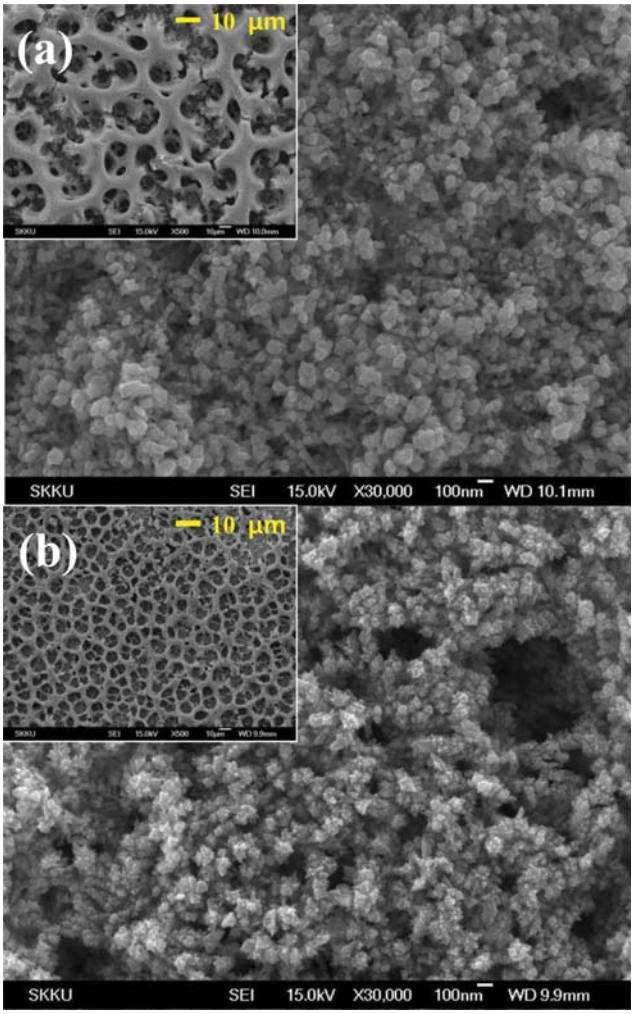

Fig. 6. SEM images of the highly porous (a) PdO electrode and (b) PdO-NiO electrode fabricated by the electro-deposition at −4 V followed by the oxidation with annealing at 500 °C in air.

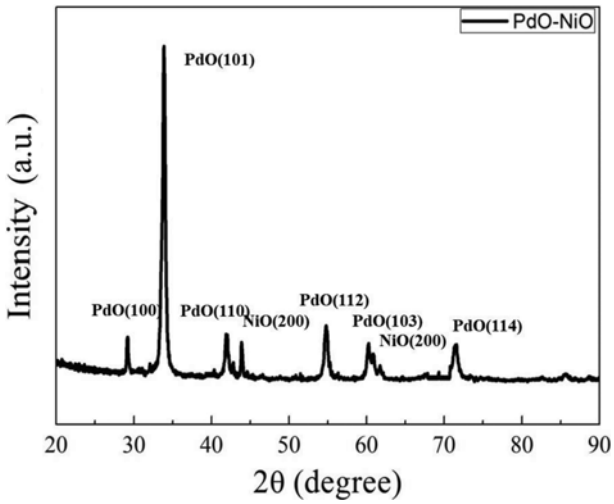

Fig. 7. XRD patterns of the prepared PdO-NiO electrode.

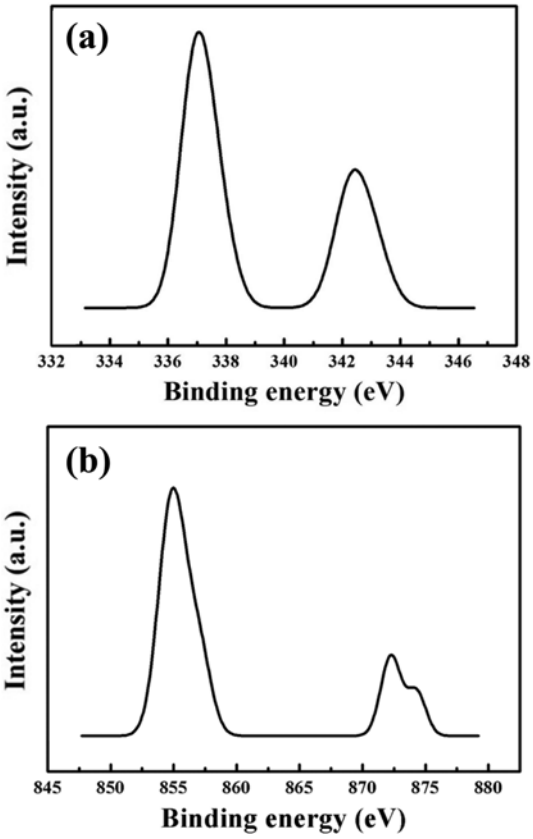

Fig. 8. XPS spectra of the (a) Pd 3d and (b) Ni 2p obtained from the PdO-NiO electrode.

sensor, highly porous PdO or PdO-NiO layer on a Pt/Ti/Si substrate was prepared through the electro-deposition followed by the oxidation with annealing in air (cf. Fig. 6). A large-surface-area was built in 0.1246 cm^2 by simple electro-deposition at high cathodic over-potential of −4 V accompanied by hydrogen bubble evolution. As noticed in Fig. 6, the bimodal morphologies are monitored. One is the nano-sized PdO or PdO-NiO aggregated structure, which provides large surface area on the sensor electrode. The other feature is the micro-sized pores produced by the hydrogen bubbles during the electro-deposition, as shown in insets of Figs. 6(a) and 6(b). These bimodal morphologies in the sensing electrode let the H_2O_2 diffuse readily into the active sites of the electrode and provide more active sites for electrochemical reduction of H_2O_2 on the electrode.

In the XRD patterns of the prepared PdO-NiO electrode, several 2θ peaks are evident at 28.65°, 34.03°, 42.17°, 54.85°, 60.51°, and 72.03° indexed to PdO (110), PdO (101), PdO (110), PdO (112), PdO (103), and PdO (114), respectively (*see* Fig. 7) [27]. The diffraction peaks of 43.85° and 62.91° are also indexed to NiO (200) and NiO (200), respectively [28,29]. No evidence of metallic Pd and Ni is presented in the XRD data, which implies that only PdO and NiO exist on the electrode. The XPS spectra shown in Fig. 8 also confirm the chemical state of PdO and NiO on the sensing electrode. In Fig. 8(a), the Pd $3d_{5/2}$ peak at 336.9 eV is the characteristic peak of PdO state [30], whereas the Ni $2p_{3/2}$ peak at 854.9 eV is assigned to NiO as noted in Fig. 8(b) [31].

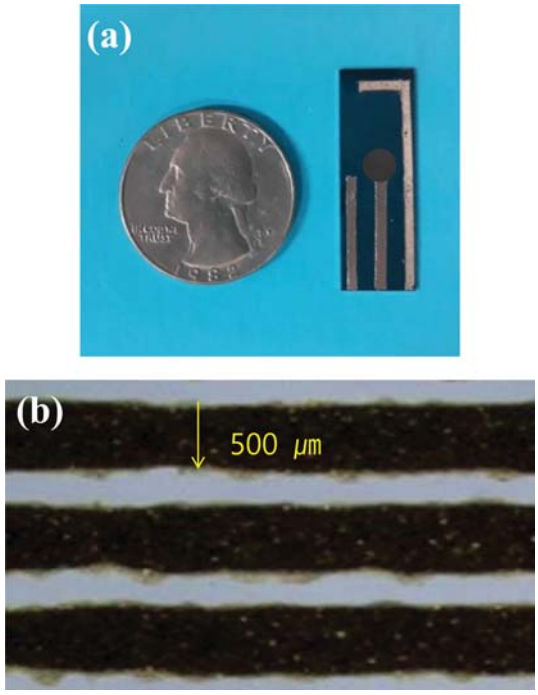

Fig. 9. The top view of (a) the fabricated microchip sensor and (b) the optical microscopic image of circuit patterns.

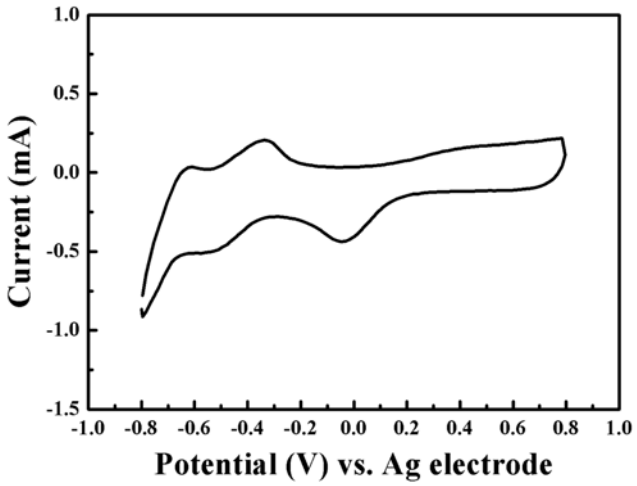

Fig. 10. Cyclic voltammograms obtained from the PdO-NiO electrodes in 0.1 M PBS (pH=7) at a scan rate of 20 mV/s.

With this highly porous PdO-NiO electrode, the microchip sensor was fabricated by photolithography as shown in Fig. 9. The 500 μm-width pattern of circuit connected to PdO-NiO working electrode was made with the paste of 33 wt% dendritic Ag@Cu powders, and the counter electrode was printed with Pt powders. Separately, the reference electrode was also made with the paste of spherical Ag powders.

The electrochemical characteristic of the prepared PdO-NiO sensor electrode was investigated in an electrolyte of 0.1 M PBS (pH=7) solution without H_2O_2 using cyclic voltammetry (CV). The potential swung in the range between −0.8 V and 0.8 V vs. Ag with a scan rate of 20 mV s^{-1}. As shown in Fig. 10, two reduction peaks on

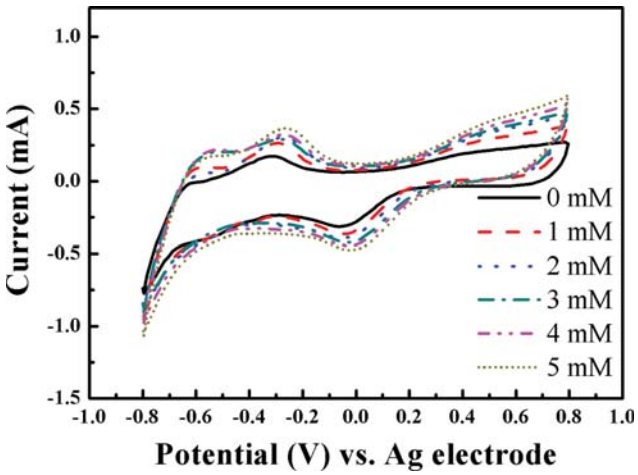

Fig. 11. Cyclic voltammograms obtained from the PdO-NiO electrode in 0.1 M PBS (pH=7) containing different concentration of H_2O_2 at scan rate of 20 mV/s.

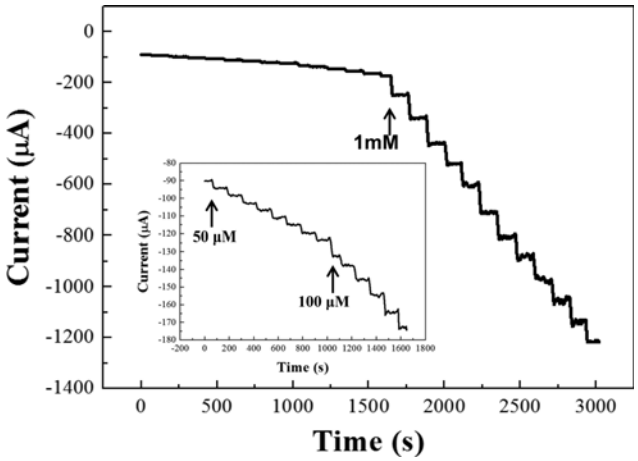

Fig. 12. Chrono-amperometric I-t curve on the PdO-NiO electrode with successive addition of 50 μM, 100 μM, and 1 mM H_2O_2 in 0.1 M PBS (pH=7) at the applied potential of −0.1 V.

the PdO-NiO appeared at −0.1 V and −0.5 V (vs. Ag), which is attributed to the reduction of palladium oxide and nickel oxide, respectively. Especially, the reduction peak of palladium oxide was believed to be caused by electro-reduction of PdO_2 to PdO.

With the addition of H_2O_2 in 0.1 M PBS electrolyte, the cathodic-current intensity at −0.1 V increases, whereas the reduction current at −0.5 V does not change that much, as shown in Fig. 11. Increase in cathodic-current intensity at −0.1 V is due to greater reduction of the additional PdO_2, which is additionally generated by the addition of H_2O_2. The related electrochemical reactions of the H_2O_2 sensing on PdO are described as follows:

$$PdO+H_2O_2 \rightarrow PdO_2+H_2O \quad (9)$$

$$PdO_2+H_2O+2e^- \rightarrow PdO+2OH^- \quad (10)$$

Note that the NiO is not incorporated into the reaction directly. The effect of NiO on the electrochemical reaction of PdO will be discussed below (*vide infra*).

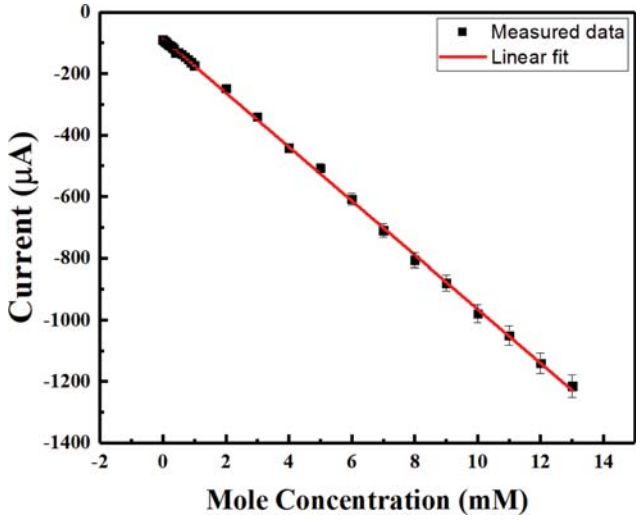

Fig. 13. The amperometric calibration curve (S/N=3) with H_2O_2 concentration between 50 μM and 13 mM detected with the PdO-NiO electrode.

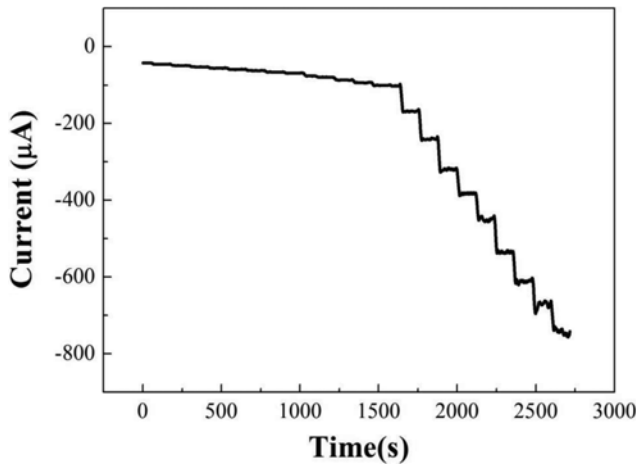

Fig. 14. Chrono-amperometric I-t curve on the PdO electrode with successive addition of 50 μM, 100 μM and 1 mM H_2O_2 in 0.1 M PBS (pH=7) at the applied potential of −0.1 V.

The typical chrono-amperometric I-t curve of Fig. 12 was measured on the highly porous PdO-NiO sensor electrode with successive additions of 50 μM, 100 μM, and 1 mM H_2O_2 in well-stirred electrolyte of 0.1 M PBS (pH=7) at the applied potential of −0.1 V and 25 °C, where a typical step-wise response is evident as the addition of different H_2O_2 concentrations. The dynamic range with linear response was from 50 μM to 13 mM, in which a correlation-coefficient of R^2 was 0.99951 and standard deviation was 2.1% as plotted in Fig. 13. The sensitivity of PdO-NiO sensor exhibits 641.75 μA mM^{-1} cm^{-2}, whereas the detection limit is 7.7 μM at a signal-to-noise ratio (S/N) of 3. In comparison with the sensitivity (508.813 μA mM^{-1} cm^{-2}) of PdO sensor electrode, the PdO-NiO electrode shows a higher sensitivity than that of PdO, even when they are prepared by the same electro-deposition and annealing steps (cf. Fig. 12 and Fig. 14). Table 3 shows the comparison of the analyti-

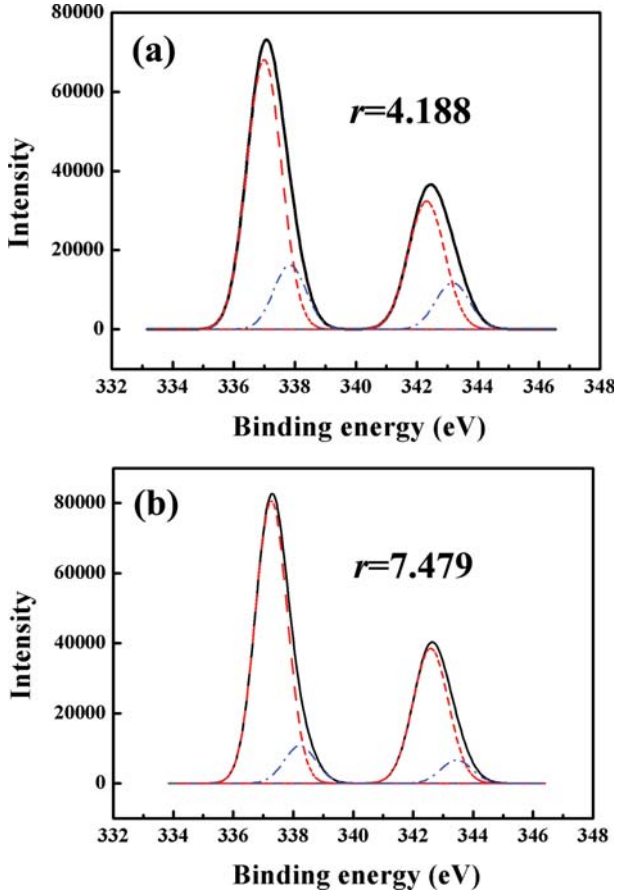

Fig. 15. XPS spectra of (a) PdO electrode after the reduction of 5 mM H_2O_2 and (b) PdO-NiO electrode after the reduction of 5 mM H_2O_2.

Table 3. Comparison of the analytical performance of some hydrogen peroxide sensors

Sensors	Linear range (mM)	Sensitivity	Detection limit (μM)	Reference
Ag nanowire array	0.1-3.1		29.2	[32]
Nafion-PB-MWCNTs/SPCE-IL	0.005-1.645	436 μA mM^{-1} cm^{-2}		[33]
Inkjet printed Ti_3C_2-GO electrode	0.002-1		1.95	[34]
Stamped multilayer graphene laminate electrode		64 nA mM^{-1} cm^{-2}	1.91	[35]
Platinum treated graphene laminate electrode		16.5 nA mM^{-1} cm^{-2}	1.98	[35]
Inkjet printed Ag electrode	0.1-6.8	287 μA mM^{-1} cm^{-2}	5.0	[36]
Our works	0.05-13	641.75 μA mM^{-1} cm^{-2}	7.7	

cal performance of some hydrogen peroxide sensors. A microchip sensor exhibits high linear range and sensitivity compared with other printed electrode and H_2O_2 sensors. Also compared with other electrodes, working, reference, counter electrode in microchip sensor were fabricated, although the working electrode was fabricated in other references.

To elucidate the effect of NiO on the sensing performance of PdO, additional XPS analyses were conducted, which are presented in Fig. 15. The PdO and PdO-NiO electrode surfaces were monitored with XPS after the electrochemical reduction of 5 mM H_2O_2. The PdO state is evident at 337.0 eV and 342.3 eV, which is Pd $3d_{5/2}$ and Pd $3d_{3/2}$ peak of PdO, respectively. The PdO_2 is also monitored at 338.1 eV and 343.4 eV, which are shifted to higher binding energy due to the further oxidation from PdO into PdO_2. As above mentioned, H_2O_2-sensing mechanism of Eqs. (9) and (10), the PdO_2 reacted with H_2O_2 and electron, producing PdO and OH^-. When the peak intensity ratio (r) is defined as following Eq. (11), therefore, it indicates the relative amount of PdO_2 reduced into PdO for the electrochemical reduction of 5 mM of H_2O_2:

$$r = \frac{\text{peak intensity of PdO}}{\text{peak intensity of PdO}_2} \tag{11}$$

As shown in the de-convoluted XPS spectra of Figs. 15(a) and 15(b), the peak intensity ratio (r) of PdO-NiO is 7.479, which is much bigger than 4.188 of PdO. It means that more PdO_2 is reduced to PdO on the PdO-NiO electrode than on the PdO electrode. Considering that the NiO itself is not incorporated into the electrochemical reduction path of H_2O_2 sensing, the NiO in PdO-NiO electrode plays a role as electron donor in reaction Eq. (10), in which the PdO_2 is reduced to the PdO.

Furthermore, the selectivity of the sensor was also evaluated by the chrono-amperometry measurements on the prepared PdO-NiO electrode responding to the addition of several other substances. As shown in Fig. 16, clear step-wise responses on increase of reduction current were observed for each time of the 0.5 mM H_2O_2 addition, whereas the changes with the addition of 0.5 mM of uric acid (UA), glucose, dopamine hydrochloride (DA), and ascorbic acid (AA) were negligible. The fabricated PdO-NiO sensor in this work responds selectively to H_2O_2 addition. The long-term stability of the fabricated electrode was also tested after the storage of four weeks at room temperature in air. It was found that the electrode records 97.78% of its original current intensity when it is sensing the 0.5 mM H_2O_2, which represents its high stability.

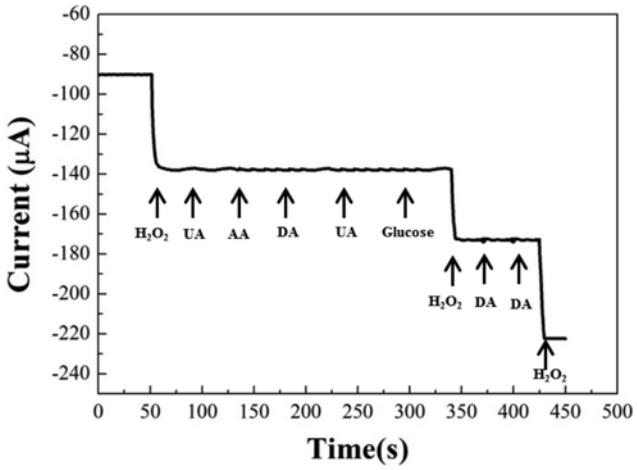

Fig. 16. Typical steady-state response of the PdO-NiO electrode to successive injection of 0.5 mM of H_2O_2, 0.5 mM of UA, 0.5 mM of glucose, 0.5 mM of AA, and 0.5 mM of DA in 0.1 M PBS (pH=7) at the applied potential of −0.1 V.

CONCLUSION

We have fabricated a small-sized pattern microchip of H_2O_2 sensor using highly porous PdO-NiO working electrode, which is built with the electro-deposition accompanied by the hydrogen-bubble evolution at high cathodic over-potential of −4 V. In circuit patterning and formation of the electrode, the photolithography process was applied using the photosensitive paste containing the metal fillers of dendritic Ag-coated Cu powders. In UV photolithography, increasing the amount of dendritic powder enhanced body resistivity because it improved networking. The high-surface-area porous PdO-NiO electrode exhibited outstanding performance for H_2O_2 detection with high sensitivity of 641.75 μA mM^{-1} cm^{-2} in a dynamic range between 50 μM and 13 mM. This excellence in sensitivity was achieved not only simply by the increase of surface area but also by the addition of NiO, which plays a favorable role in the H_2O_2-reduction as an electron donor providing more electrons in the reaction path of PdO_2 into PdO. We also confirmed that this PdO-NiO sensor electrode presents excellent selectivity and stability. These methods to fabricate small-sized pattern microchip sensor, with high detection range and sensitivity, can be an excellent technique in sensing applications.

ACKNOWLEDGEMENT

This research was supported by the National Research Foundation of Korea grant funded by the Korea government (MSIT) [Grant number NRF-2019R1A2B5B01070383].

REFERENCES

1. S. Chen, R. Yuan, Y. Chai and F. Hu, *Microchim. Acta*, **180**, 15 (2012).
2. S. Cinti, F. Arduini, D. Moscone, G. Palleschi and A. J. Killard, *Sensors (Basel)*, **14**, 14222 (2014).
3. M. Mujeeb-U-Rahman, D. Adalian and A. Scherer, *J. Nanotechnology,* **2015**, 1 (2015).
4. A. Moya, G. Gabriel, R. Villa and F. J. del Campo, *Curr. Opin. Electrochem.*, **3**, 29 (2017).
5. G. Hughes, K. Westmacott, K. C. Honeychurch, A. Crew, R. M. Pemberton and J. P. Hart, *Biosensors*, **6**, 29 (2016).
6. R. A. S. Couto, J. L. F. C. Lima and M. B. Quinaz, *Talanta*, **146**, 801 (2016).
7. V. Katseli, A. Economou and C. Kokkinos, *Electrochem. Commun.*, **103**, 100 (2019).
8. S. Kim, J.-h. Park, K. Kang, C.-O. Park and I. Park, *J. Micromech. Microeng.*, **25**, 015002 (2015).
9. C. K. Kim, G.-J. Lee, M. K. Lee and C. K. Rhee, *Powder Technol.*,

263, 1 (2014).
10. H. T. Hai, J. G. Ahn, D. J. Kim, J. R. Lee, H. S. Chung and C. O. Kim, *Surf. Coat. Technol.*, **201**, 3788 (2006).
11. H. Nishikawa, S. Mikami, K. Miyake, A. Aoki and T. Takemoto, *Mater. Trans.*, **51**(10), 1785 (2010).
12. S. S. Djokić and N. S. Djokić, *J. Electrochem. Soc.*, **158**, D204 (2011).
13. J. Liu and X. Zeng, *J. Mater. Res.*, **27**, 1853 (2012).
14. K. Zhuo, C. Y. An, P. K. Kannan, N. Seo, Y.-S. Park and C.-H. Chung, *Korean J. Chem. Eng.*, **34**(9), 1483 (2017).
15. J. Zhao, D. Zhang and J. Zhao, *J. Solid State Chem.*, **184**, 2339 (2011).
16. Y.-S. Park, C. Y. An, P. K. Kannan, N. Seo, K. Zhuo, T. K. Yoo and C.-H. Chung, *Appl. Surf. Sci.*, **389**, 865 (2016).
17. Y. Zhang and G. S. Wilson, *J. Electroanal. Chem.*, **345**, 253 (1993).
18. S. Zhang, L. Han, C. Hou, C. Li, Q. Lang, L. Han and A. Liu, *J. Electroanal. Chem.*, **742**, 84 (2015).
19. T. Zhang, R. Yuan, Y. Chai, W. Li and S. Ling, *Sensors (Basel)*, **8**, 5141 (2008).
20. P. Saha, A. Maharajan, P. K. Dikshit and B. S. Kim, *Korean J. Chem. Eng.*, **36**(12), 2143 (2019).
21. R. Ojani, J.-B Raoof and B. Norouzi, *Int. J. Electrochem. Sci.*, **7**, 1852 (2012).
22. L. Zhu, Y. Zheng and J. Jian, *Ionics*, **21**, 2919 (2015).
23. J. Lee, D. Sharma, Y. Lim and H. Shin, *Sens. Actuators B: Chem.*, **267**, 467 (2018).
24. J. Kim, S. Y. Oh, J. Y. Park and Y. Kim, *Korean J. Chem. Eng.*, **33**(1), 344 (2016).
25. C. Y. An, K. Zhuo, W.-J. Kim and C.-H. Chung, *Sens. Actuators B: Chem.*, **213**, 329 (2015).
26. F. M. Smits, *Bell Syst. Tech. J.*, **37**(3), 711 (1958).
27. Y. Q. Zhang, W. X. Yang, Y. Z. Wang, J. B. Jia and J. G. Wang, *Microchim. Acta*, **180**, 1085 (2013).
28. S. Vijayakumar, S. Nagamuthu and G. Muralidharan, *ACS Appl. Mater. Interfaces*, **5**, 2188 (2013).
29. B. Ren, M. Q. Fan, Q. Liu, J. Wang, D. L. Song and X. F. Bai, *Electrochim. Acta*, **92**, 197 (2013).
30. C.-S. Chen and F.-M. Pan, *J. Power Sources*, **208**, 9 (2012).
31. M. M. Barroso-Quiroga and A. E. Castro-Luna, *Int. J. Hydrogen Energy*, **35**, 6052 (2010).
32. E. Kurowska, A. Brzózka, M. Jarosz, G. D. Sulka and M. Jaskuła, *Nanotechnology*, **23**, 7 (2012).
33. X. Zhu, X. Niu, H. Zhao and M. Lan, *Sens. Actuators B: Chem.*, **195**, 274 (2014).
34. J. Zheng, J. Diao, Y. Jin, A. Ding, B. Wang, L. Wu, B. Weng and J. Chen, *J. Electrochem. Soc.*, **165**, 5 (2018).
35. L. R. Stromberg, J. A. Hondred, D. Sanborn, D. Mendivelso-Perez, S. Ramesh, I. V. Rivero, J. Kogot, E. Smith, C. Gomes and J. C. Claussen, *Microchim. Acta*, **186**, 533 (2019).
36. L. Shi, M. Layani, X. Cai, H. Zhao, S. Magdassi and M. Lan, *Sens. Actuators B: Chem.*, **256**, 938 (2018).